

Remote sensing vegetation indices enhance understanding of the coupling of terrestrial ecosystem evapotranspiration and photosynthesis on a global scale

Yun Bai¹, Sha Zhang², Jiahua Zhang³, Shanshan yang², Jingwen Wang², Enzo Magliulo⁴, Luca Vitale⁵, and Yanchuang Zhao⁶

¹Qingdao University

²Institute of Remote Sensing and Digital Earth, Chinese Academy of Sciences; University of Chinese Academy of Sciences

³Institute of Remote Sensing and Digital Earth, Chinese Academy of Sciences, Beijing, China

⁴CNR ISAFoM

⁵CNR Institute for Mediterranean Agricultural and Forest Systems

⁶College of Information Science and Engineering, Henan University of Technology, 450001 Zhengzhou, PR China; Instituto Multidisciplinar para el Estudio del Medio "Ramón Margalef," Universidad de Alicante, 03690 San Vicente del Raspeig, Alicante, Spain.

November 28, 2022

Abstract

The current approaches have known limitations to understanding the coupling of terrestrial ecosystem evapotranspiration (ET) and photosynthesis (referred to as gross primary productivity, GPP). To better characterize the relationship between ET and GPP, we developed a novel remote sensing (RS)-driven approach (RCEEP) based on the underlying water use efficiency (uWUE). RCEEP partitions transpiration (T) from ET using a RS vegetation index (VI)-derived ratio of T to ET (VI-fT) and then links T and GPP via RS VI-derived Gc (VI-Gc) rather than leaf-to-air vapor pressure difference. RCEEP and other two uWUE versions (VI-T or VI-G), which only incorporate VI-fT or VI-Gc, were evaluated and compared with the original uWUE model in terms of their performances (Nash-Sutcliffe efficiency, NSE) in estimating GPP from ET over 180 flux sites covering 11 biome types over the globe. Results revealed better performances of VI-T and VI-G compared to the original uWUE, implying remarkable contributions of VI-fT and VI-Gc to a more meaningful relationship between ET and GPP. RCEEP yielded the best performances with a reasonable mean NSE value of 0.70 (0.76) on a daily (monthly) scale and across all biome types. Further comparisons of RCEEP and approaches modified from recent studies revealed consistently better performances of RCEEP and thus, positive implications of introducing VI-fT and VI-Gc in bridging ecosystem ET and GPP. These results are promising in view of improving or developing algorithms on coupled estimates of ecosystem ET and GPP and understanding the GPP dynamics concerning ET on a global scale.

Hosted file

supporting-information-tab_in_template.docx available at <https://authorea.com/users/546665/articles/606884-remote-sensing-vegetation-indices-enhance-understanding-of-the-coupling-of-terrestrial-ecosystem-evapotranspiration-and-photosynthesis-on-a-global-scale>

Hosted file

supporting-information-text_in_template.docx available at <https://authorea.com/users/546665/articles/606884-remote-sensing-vegetation-indices-enhance-understanding-of-the-coupling-of-terrestrial-ecosystem-evapotranspiration-and-photosynthesis-on-a-global-scale>

1 **Remote sensing vegetation indices enhance understanding of the**
2 **coupling of terrestrial ecosystem evapotranspiration and**
3 **photosynthesis on a global scale**

4
5 **Bai Yun^{1*}, Zhang Sha¹, Zhang Jiahua^{1,2}, Wang Jingwen^{2,3}, Yang Shanshan²,**

6 **Vincenzo Magliulo⁴, Luca Vitale⁴, Zhao Yanchuang^{5,6}**

7 1 Centre for Remote Sensing and Digital Earth, College of Computer Science and Technology,
8 Qingdao University, 266071 Qingdao, China.

9 2 Key Laboratory of Digital Earth Science, Institute of Remote Sensing and Digital Earth,
10 Aerospace Information Research Institute Chinese Academy of Sciences, 100094 Beijing, China.

11 3 EMMAH UMR 1114, INRAE, 84914 Avignon, France

12 4 CNR Institute for Mediterranean Agricultural and Forest Systems, Via Patacca, 85, Ercolano
13 (Napoli), Italy

14 5 College of Information Science and Engineering, Henan University of Technology,
15 450001 Zhengzhou, PR China

16 6 Instituto Multidisciplinar para el Estudio del Medio “Ramón Margalef,” Universidad de
17 Alicante, 03690 San Vicente del Raspeig, Alicante, Spain.

18 * Corresponding author: Bai Yun, Email: baiyun@qdu.edu.cn

19

20 Key points:

21 ● We proposed a novel remote sensing approach to coupling ecosystem
22 evapotranspiration (ET) and photosynthesis (GPP) (RCEEP)

23 ● RCEEP performed reliably and better than existing methods as to
24 reproducing GPP from ET on a global scale

25 ● Remote sensing vegetation indices used in RCEEP remarkably
26 contribute to the more meaningful relationship between ET and GPP

27

28 **Abstract**

29 The current approaches have known limitations to understanding the coupling of terrestrial
30 ecosystem evapotranspiration (ET) and photosynthesis (referred to as gross primary productivity,
31 GPP). To better characterize the relationship between ET and GPP, we developed a novel
32 remote sensing (RS)-driven approach (RCEEP) based on the underlying water use efficiency
33 (uWUE). RCEEP partitions transpiration (T) from ET using a RS vegetation index (VI)-derived
34 ratio of T to ET ($VI-f_T$) and then links T and GPP via RS VI-derived G_c ($VI-G_c$) rather than
35 leaf-to-air vapor pressure difference. RCEEP and other two uWUE versions (VI-T or VI-G),
36 which only incorporate $VI-f_T$ or $VI-G_c$, were evaluated and compared with the original uWUE
37 model in terms of their performances (Nash-Sutcliffe efficiency, NSE) in estimating GPP from
38 ET over 180 flux sites covering 11 biome types over the globe. Results revealed better
39 performances of VI-T and VI-G compared to the original uWUE, implying remarkable
40 contributions of $VI-f_T$ and $VI-G_c$ to a more meaningful relationship between ET and GPP.
41 RCEEP yielded the best performances with a reasonable mean NSE value of 0.70 (0.76) on a
42 daily (monthly) scale and across all biome types. Further comparisons of RCEEP and approaches
43 modified from recent studies revealed consistently better performances of RCEEP and thus,
44 positive implications of introducing $VI-f_T$ and $VI-G_c$ in bridging ecosystem ET and GPP. These
45 results are promising in view of improving or developing algorithms on coupled estimates of
46 ecosystem ET and GPP and understanding the GPP dynamics concerning ET on a global scale.

47 **Plain Language Summary**

48 Evapotranspiration and photosynthesis processes of land ecosystems are mutually
49 affected. Reasonable representations of the relationship between the two processes

50 are important for us to understand the way the environment changes under the
51 background of climate change. However, existing models that represent the
52 evapotranspiration-photosynthesis relationship have several known limitations. To
53 better characterize the evapotranspiration-photosynthesis relationship, we developed
54 a novel approach to bridging evapotranspiration and photosynthesis based on
55 vegetation information remotely sensed by satellite. We found that the novel
56 approach could present a more meaningful relationship between ecosystem
57 evapotranspiration and photosynthesis than the existing methods over the globe. This
58 finding reveals positive implications of introducing remotely sensed vegetation
59 information in reasonably representing the evapotranspiration-photosynthesis
60 relationship. Moreover, the novel approach we developed paves a way for more
61 insightful understanding of the evapotranspiration and photosynthesis of land
62 ecosystems and their relationship.

63

64 **Keywords:** Remote sensing; Vegetation indices; Evapotranspiration; Gross primary
65 productivity; Terrestrial ecosystems; Global

66 **1 Introduction**

67 Terrestrial ecosystem evapotranspiration (ET) and photosynthesis (referred to as gross
68 primary productivity, GPP) play important roles in land-atmosphere material and energy
69 exchanges. The two processes are also closely coupled (Beer et al., 2009; Zhou et al., 2014) due
70 to the dominating role of transpiration (T) in evapotranspiration (ET) (Jasechko et al., 2013; Li et

71 al., 2019; Stoy et al., 2019) and the combined relationship between T and carbon assimilation (A)
72 due to the common stomatal pathway (Cowan and Farquhar, 1977; Medlyn et al., 2011) over
73 global terrestrial biomes. Therefore, the knowledge of the quantitative correlation between
74 ecosystem ET and GPP can provide insightful views on modeling and understanding the earth
75 systems. However, the relationship between ET and GPP on an ecosystem level is still only
76 partly understood (Boese et al., 2017), so that more robust and general approaches are urgently
77 needed.

78 Established theories to express the quantitative relationship between T and A are available
79 from leaf to ecosystem-level (Beer et al., 2009; Medlyn et al., 2011; Zhou et al., 2014).
80 Representing stomatal behavior is the key to couple the water and carbon exchanges between the
81 plant and environment as both water loss and carbon up-taking are dominated by stomata
82 (Cowan and Farquhar, 1977; Ball et al., 1987; Collatz et al., 1991; Leuning, 1995). The
83 long-standing theory of optimal stomatal behavior (TOSB) (Cowan and Farquhar, 1977) and the
84 experiment of Mott and Parkhurst (1991) indicate a direct response of stomatal conductance (g_s)
85 to leaf-to-air vapor pressure difference (D). Analytical stomatal conductance model of Medlyn et
86 al. (2011) following this TOSB consistently demonstrated the response of g_s to \sqrt{D} and thus
87 the dependence of the coupling of T and A on D on a leaf-level (see also Appendix C). The
88 importance of D in coupling ecosystem-level ET and GPP was also widely recognized (Beer et
89 al., 2009; Zhou et al., 2014, 2015; Cheng et al., 2017). Assuming steady-state environmental
90 conditions with a constant value of c_i/c_a allows for bridging ecosystem-level T and A (i.e., GPP)
91 via the inherent water use efficiency (IWUE) (Beer et al., 2009), which is defined as $IWUE =$
92 $GPP \cdot D/T = c_a(1 - c_i/c_a)/1.6$ (see also Appendix C), where c_i and c_a denotes the inner-leaf

93 and ambient CO₂ partial pressure, D is substituted by VPD, and T is approximated by ET. To
94 enhance the relationship between T and GPP under a changing environment, Zhou et al. (2014)
95 approximated $(1 - c_i/c_a)$ as a proportion to \sqrt{D} as indicated by Lloyd and Farquhar (1994)
96 and introduced the concept of Underlying Water Use Efficiency (uWUE) to link T and GPP (see
97 also Section 2.1). uWUE can lead to a more reliable relationship between ecosystem T (using ET
98 as a surrogate) and GPP than did IWUE under changing environments, i.e., $uWUE \cdot T =$
99 GPP/\sqrt{D} , which is robust from hourly to yearly scales (Zhou et al., 2014, 2015).

100 However, the ecosystem-level relationships between ET and GPP over global terrestrial
101 biomes are biased by the presence of the evaporation components of ET, e.g. soil evaporation
102 (E_s), and the difficulties to access the true value of D . uWUE uses ET to approximate T (Zhou et
103 al., 2014, 2015), an approach prone to errors, since T is not a constant fraction of ET (Wang et al.,
104 2014; Wei et al., 2017; Lian et al., 2018; Stoy et al., 2019). Multiple studies revealed variable
105 contributions of T or E_s to ET over global biomes (Cavanaugh et al., 2011; Gu et al., 2018; Lian
106 et al., 2018; Perez-Priego et al., 2018; Li et al., 2019). As E_s is free from the effect of stomatal
107 conductance (g_s) which is in turn regulated by D (Leuning, 1995; Medlyn et al., 2011), uWUE
108 may fail to represent the relationship between ET and GPP of ecosystems with changing E_s/ET
109 values. Since the true value of D is difficult to be obtained, uWUE uses VPD as an approximate
110 (Zhou et al., 2014, 2015). However, VPD significantly deviates from D due to significant
111 temperature differences between leaf (or canopy) and ambient air (Friedl, 1995; Nelson and
112 Bugbee, 2015), under drought (Almeida, 1986; Olufayo et al., 1993), as well as under
113 well-watered conditions (Jackson et al., 1981; Idso, 1982; Idso et al., 1982a; Idso et al., 1982b).

114 The above issues relevant for a successful implementation of the uWUE approach can be

115 addressed using remote sensing (RS) techniques. Efforts devoted to partition T from ET revealed
116 a great impact of vegetation information that can be remotely sensed on the value of E_s/ET or
117 T/ET (denoted as f_T thereafter) (Wang et al., 2014; Zhou et al., 2016; Wei et al., 2017; Gu et al.,
118 2018; Perez-Priego et al., 2018). For example, Wang et al. (2014) and Wei et al. (2017) showed
119 tight correlations between the value of f_T and vegetation leaf area index (LAI). On the other end,
120 the problem connected with a proper assessment of D was rarely focused (Drake et al., 2017; Li
121 et al., 2019), due to the difficulty to acquire accurate canopy temperature or transpiration
122 information over broad regions or long terms. Li et al. (2019) and Drake et al. (2017) used VPD_l
123 instead of VPD to approximate D ; however, it should be noted that VPD_l is also affected by soil
124 evaporation. In the uWUE approach, D was harnessed for representing the stomatal effects on
125 the photosynthesis-transpiration relationship. On the other hand, using g_s rather than D to
126 couple ET and GPP could be more straightforward, while canopy level g_s (canopy conductance,
127 denoted as G_c) can be reasonably characterized by RS vegetation indices (VIs) (Yebra et al., 2013;
128 Bai et al., 2017).

129 uWUE presents a concise and effective approach to coupling ecosystem ET and GPP but its
130 effectiveness is limited by the sensible differences between ET and T , and VPD and D . The two
131 issues can be potentially addressed by application of RS VIs. We exploited RS-driven approaches
132 to coupling ecosystem ET and GPP with three main objectives:

- 133 (1) Modify the uWUE approach by linking T and GPP via G_c rather than D ;
- 134 (2) Propose a novel RS-driven approach to coupling ecosystem ET and GPP based on the
135 modified uWUE as mentioned in (1) by characterizing f_T and G_c using RS VIs;
- 136 (3) Compare the performances between the RS-driven approach, two uWUE-derived

137 versions which only use RS-retrieved f_T or G_c , and the original version of uWUE,
138 concerning reproducing daily and monthly-scale GPP from ET over 180 flux sites
139 covering multiple biome types over the globe.

140 (4) Furtherly explore the differences in performance between the novel RS-driven approach
141 and other methods modified from recent studies, which aimed to reasonably partition T
142 from ET or link ET and GPP on an ecosystem level, concerning estimating GPP from
143 ET on a daily scale and over the flux sites used in (3).

144 **2 Materials and Methods**

145 2.1 An overview of the underlying water use efficiency

146 The underlying water use efficiency (uWUE) proposed by Zhou et al. (2014) provides an
147 easy approach to coupling ecosystem-level T and A and is robust from hourly to yearly scales
148 (Zhou et al., 2015). The uWUE is derived from Inherent Water Use Efficiency (IWUE) (Beer et
149 al., 2009), which incorporates D to link A and T under the steady-state condition with a
150 constant c_i/c_a value. Zhou et al. (2014) developed uWUE by integrating the expressions of A
151 and T following the Fick's law (Beer et al., 2009; Nobel, 2009) and assuming c_i/c_a , to be
152 proportional to \sqrt{D} (Lloyd and Farquhar, 1994), on the basis of the theory of optimal stomatal
153 behavior (TOSB) (Cowan and Farquhar, 1977). The following equation represents the
154 relationship between T and A through uWUE.

$$155 \quad w \cdot T = A \cdot \sqrt{D}, \quad (1)$$

156 where w denotes the underlying water use efficiency (uWUE: $\mu\text{mol C (mol H}_2\text{O)}^{-1} \text{ kPa}^{0.5}$),
157 which is supposed to remain constant for a specific biome (Zhou et al., 2014); T is the

158 transpiration measured in $\text{mol m}^{-2} \text{s}^{-1}$; and D represents the leaf-to-air vapor pressure deficit
159 measured in kPa.

160 At the ecosystem level, Eq.(1) can be expressed as the following equation:

$$161 \quad w \cdot T = \text{GPP} \cdot \sqrt{D}, \quad (2)$$

162 where T is approximated by ET in Zhou et al. (2014). D is not an easily acquired factor on a
163 regional scale, therefore Zhou et al. (2014) and Zhou et al. (2015) used VPD to approximate D ,
164 assuming leaf temperature is the same as air temperature, a hypothesis widely accepted (Medlyn
165 et al., 2011; Zhang et al., 2016; Boese et al., 2017; Medlyn et al., 2017). However, VPD may fail
166 to properly approximate D , as considerable differences in temperature between leaf and air are
167 commonly found (Jackson et al., 1981; Idso et al., 1982b; Almeida, 1986; Olufayo et al., 1993;
168 Nelson and Bugbee, 2015), which may induce substantial uncertainties in representing the
169 transpiration-photosynthesis relationship.

170 2.2 Remote sensing-driven approach to Coupling Ecosystem Evapotranspiration and 171 Photosynthesis (RCEEP)

172 2.2.1 Linking ecosystem ET and GPP via canopy conductance

173 Stomata is the main pathway for water loss and carbon uptake of plant leaves (Cowan and
174 Farquhar, 1977; Beer et al., 2009; Medlyn et al., 2011), and D (Eq.(2)) in the uWUE approach is
175 harnessed for representing the effect of stomatal conductance on the transpiration-photosynthesis
176 relationship. Therefore, a more straightforward approach to coupling ET and GPP is to represent
177 their relationship in terms of the g_s (G_c on a canopy or ecosystem level). G_c and D are linked
178 by the following relationship, according to Fick's law (Beer et al., 2009; Nobel, 2009):

179
$$T = \frac{D \cdot G_c}{P_a}, \quad (3)$$

180 where G_c is measured in $\text{mol m}^{-2} \text{s}^{-1}$; P_a is the atmosphere pressure (kPa). We can integrate
 181 Eq.(2) with (3) to eliminate D and derive the following equations to represent the relationship
 182 between ET and GPP in terms of G_c .

183
$$\text{GPP} = w \cdot \sqrt{\frac{T \cdot G_c}{P_a}}, \quad (4)$$

184
$$T = f_T \cdot \text{ET}, \quad (5)$$

185 where f_T denotes the proportion of vegetation transpiration, T , in ET.

186 2.2.2 Representing G_c and f_T using RS VIs

187 2.2.2.1 G_c in terms of EVI

188 Satellite-retrieved near-infrared vegetation indices are capable of characterizing the
 189 seasonal variations in G_c . (Zhang et al., 2009; Yebra et al., 2013; Bai et al., 2018). In this study,
 190 we incorporate a simple relationship between G_c and satellite-retrieved enhanced vegetation
 191 index (EVI).

192
$$G_c = k_G \cdot \text{sEVI}, \quad (6)$$

193
$$\text{sEVI} = \max(\text{EVI} - \text{EVI}_{\text{soil}}, 0) \cdot (1 - p) + p, \quad (7)$$

194 where k_G is a multiplier scaling sEVI to G_c ; sEVI denotes the scaled EVI value; EVI_{soil}
 195 denotes the EVI value of soil; p denotes the minimum value of sEVI and is fixed to 0.01 in this
 196 study. While Yebra et al. (2013) proposed a nonlinear correlation, we propose a linear
 197 relationship between EVI and G_c , because we found EVI could linearly correlate to
 198 $\text{GPP}/(C_a \cdot \sqrt{\text{VPD}})$, which is scaled with G_c , as indicated by Medlyn et al. (2011). We linearly
 199 fitted $\text{GPP}/(C_a \cdot \sqrt{\text{VPD}}) = \text{slope} \times \text{sEVI}$ to derive EVI_{soil} using the least-square method

200 along with daily tower-derived GPP of 180 flux sites (see also Section 2.4.1), and the value of
201 EVI_{soil} turned out to be 0.10 ($R^2 = 0.47$).

202 Canopy conductance, G_c , is also regulated by many environmental parameters, e.g. air
203 temperature, solar radiation, and leaf water potential, in addition to EVI, and thus may be more
204 reasonably estimated by a more complicated formulation of G_c , in which these factors were
205 accounted for. Here, we considered such a formulation, $G_c = k \cdot (\text{sEVI} \cdot \phi)^b$ (see also Text S1),
206 where k and b are empirical coefficients and ϕ denotes the surface wetness, calculated as the
207 ratio of actual ET to Priestley-Taylor equation derived ET potential (Priestley and Taylor, 1972).
208 Previous studies have found ϕ tightly and nonlinearly correlated to surface conductance
209 (Baldocchi and Xu, 2007; Ryu et al., 2008; Ma et al., 2015). Therefore, ϕ can effectively
210 represent the environmental constraints on G_c , and the term $k \cdot (\text{sEVI} \cdot \phi)^b$ could be a better
211 approximation for G_c than $k_G \cdot \text{sEVI}$. However, we found that such a G_c formulation showed
212 no tendencies to facilitate a more meaningful relationship between ET and GPP (see also Section
213 4.2 and Text S1), as compared with that simply estimated using Eq.(6).

214 2.2.2.2 f_T in terms of NDVI

215 Ecosystem ET is by definition different from T as the contribution of soil evaporation is in
216 most cases significant (Cavanaugh et al., 2011; Gu et al., 2018; Perez-Priego et al., 2018; Li et al.,
217 2019). T could be partitioned from ET based on Eq. (5), where f_T is unknown. Efforts have been
218 devoted to estimate f_T and indicated the potential of resolving this issue using remote sensing
219 techniques (Cavanaugh et al., 2011; Zhou et al., 2016; Gu et al., 2018; Perez-Priego et al., 2018;
220 Li et al., 2019). In this study, we evaluate a simple RS approach to approximating f_T . As ET is

221 primarily forced by solar radiation (Wang et al., 2010; Boese et al., 2017), we assume f_T is
222 proportional to the Fraction of Absorbed Photosynthetically Active Radiation (f_{PAR}) (Sims et al.,
223 2005) and estimate the former as follows:

$$224 \quad f_T = k_T \cdot f_{PAR} = k_T \cdot (1.24 \times NDVI - 0.168), \quad (8)$$

225 where k_T denotes the ratio of f_T to f_{PAR} (dimensionless). A similar approximation was made
226 by Cheng et al. (2017), who also used f_{PAR} to approximate f_T but calculated f_{PAR} in terms of
227 Beer's Law along with RS-derived LAI. However, due to large uncertainties existing in
228 nowadays' LAI products (Yang et al., 2007; Jin et al., 2017), we used NDVI instead of LAI to
229 compute f_{PAR} . We symbolized f_T computed according to Eq. (8) as NDVI- f_T .

230 2.2.3 RS-driven coupling of ET and GPP

231 Integrating Eq.(4) with Eq.(6) and (8), we can derive an original formulation linking
232 ecosystem ET and GPP we termed 'Remote sensing-driven approach to Coupling Ecosystem
233 Evapotranspiration and Photosynthesis' (RCEEP), representing a novel remote sensing-driven
234 approach to coupling these two fluxes. We then compare the performances of RCEEP with the
235 original version of the uWUE (Table 1), which uses ET and VPD to approximate T and D ,
236 respectively, for calculating GPP from ET. For better clarifying how RS VIs could facilitate more
237 meaningful relationships between ET and GPP, we also evaluate two additional versions of
238 RS-based approaches modified from the uWUE. The first one, formulated following Eq.(2)
239 (VI-T in Table 1), incorporates the NDVI-derived f_T to calculate T from ET (Eq.(5) and (8)) and
240 approximates D by VPD. The second one, formulated following Eq. (4) (VI-G in Table 1), only
241 incorporates EVI- G_c (Eq. (6)) and approximate T by ET. If the use of either NDVI- f_T or EVI- G_c

242 plays a positive role in improving the coupling of ecosystem ET and GPP, then VI-T, VI-G, and
 243 RCEEP should all perform better than the uWUE, and RCEEP is supposed to perform the best.

244

245 Table 1 Analytical expression of uWUE, VI-T, VI-G, and RCEEP models.^a

Model Name	RS-derived factors considered	Formulation
uWUE	-	$GPP = w \cdot ET / \sqrt{VPD}$
VI-T	NDVI- f_T	$GPP = (w \cdot k_T) \cdot (f_{PAR} \cdot ET) / \sqrt{VPD}$,
VI-G	EVI- G_c	$GPP = (w \cdot \sqrt{k_G}) \cdot \sqrt{sEVI \cdot ET \cdot P_a^{-1}}$
RCEEP	NDVI- f_T and EVI- G_c	$GPP = (w \cdot \sqrt{k_G \cdot k_T}) \cdot \sqrt{sEVI \cdot f_{PAR} \cdot ET \cdot P_a^{-1}}$

246 2.3 Models' Calibration and Evaluation

247 Undetermined constants need to be estimated in order to numerically define the
 248 relationships linking GPP and ET according to the models presented in Table 1. These
 249 coefficients are determined by fitting each model (or equation) using the least-square method and
 250 on the basis of observed flux-derived (referred to as 'observed') daily-scale GPP (GPP_{obs}) and
 251 ET (λE_{obs}) of the flux sites described in 2.4. To avoid the confounding effect of evaporation of
 252 rainfall intercepted by the canopy, we only use data from rain-free days. Data records with
 253 $GPP_{obs} \leq 1 \mu\text{mol m}^{-2}\text{s}^{-1}$ were also removed. Each value of $w \cdot k_T$, $w \cdot \sqrt{k_G}$, and $w \cdot \sqrt{k_G \cdot k_T}$ in
 254 VI-T, VI-G, and RCEEP is treated as a single quantity. Coefficients for each model were
 255 determined by directly fitting corresponding equations and are reported in Appendix A.

256 The four approaches presented in Table 1 are evaluated by comparing GPP estimated
 257 (GPP_{est}) using these models, along with λE_{obs} and other required inputs, against the observed
 258 GPP (GPP_{obs}) of flux sites on a daily and monthly scale. Monthly GPP_{est} is not the simple
 259 average of daily estimates but was rather estimated using the fitted equations with required

260 inputs. We use data of both rainy and rain-free days for the validations. We use the
 261 Nash-Sutcliffe efficiency, NSE, (Nash and Sutcliffe, 1970; Krause et al., 2005) to measure the
 262 performances of each model (Table 1), calculated as follows:

$$263 \quad \text{NSE} = \frac{\sum_{i=1}^N (p_i - o_i)^2}{\sum_{i=1}^N (o_i - \bar{o})^2}, \quad (9)$$

264 where o_i and p_i denote observed and model-predicted values, \bar{o} the average of observed
 265 values and N represents the total number of samples. The value of the index ranges from $-\infty$ to 1
 266 (perfect fit). Large and positive NSE values relate to good performances of the model, while
 267 values lower than zero indicates that the mean of the observations would have been a better
 268 estimate than the value predicted by the model.

269 The comparisons between the four models presented in Table 1 are carried out to
 270 demonstrate the importance of $\text{NDVI-}f_T$ and $\text{EVI-}G_c$ in the RCEEP. However, considering the
 271 recent efforts to partitioning T from ET or representing more meaningful relationships between
 272 ET and GPP on an ecosystem level, it is worthwhile to clarify the differences in performances
 273 between RCEEP and approaches modified from recent studies. Therefore, we compare RCEEP
 274 with three additional approaches modified from recent works that aimed to reasonably partition T
 275 from ET or link ET and GPP on an ecosystem level. We considered three approaches modified
 276 from recent studies, (1) RCEEP incorporating f_T derived from the Priestley-Taylor Jet
 277 Propulsion Laboratory (PT-JPL) (Fisher et al., 2008; Gu et al., 2018) (RCEEP-JPL), (2) WUE
 278 and ET-based carbon uptake model (WEC) (Cheng et al., 2017), and (3) uWUE incorporating
 279 solar radiation (R_g) (uWUE- R_g) (Boese et al., 2017). Details of the three approaches can be
 280 found in Appendix D. Both RCEEP-JPL and WEC are optimized and compared with RCEEP for

281 each biome types on a daily scale; while we optimize and run RCEEP and uWUE-Rg for each
282 site on a daily scale, and the comparison between the two models is carried out on a biome level
283 in terms of the values of their performance metric (i.e., NSE) aggregated from site-scale
284 measurements. WEC considers canopy interception evaporation (E_i), however, modeling this ET
285 component is beyond the scope of this study. For a fair comparison between RCEEP,
286 RCEEP-JPL, and WEC, we used only rain-free days' data. As uWUE-Rg is designed for only
287 rain-free days (Boese et al., 2017), we also remove data of rainy days in the comparison between
288 RCEEP and uWUE-Rg.

289 2.4 Data and data processing

290 2.4.1 Flux site data

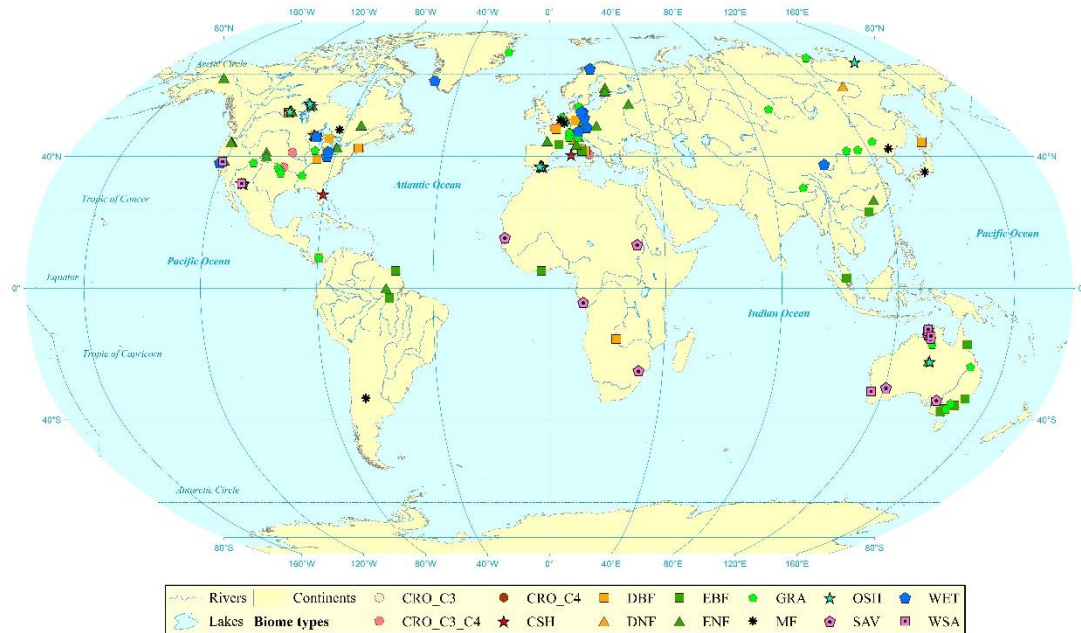
291 Site-scale observations of GPP, ET (derived from latent heat flux, λE) and required
292 meteorological data in this study were retrieved from the FLUXNET2015 Tier 2 data (available
293 at <https://fluxnet.fluxdata.org/>). This dataset provides hourly (or half-hourly), daily, weekly,
294 monthly, and yearly water, carbon and energy fluxes as well as meteorological data. All network
295 sites assess turbulent fluxes by means of the eddy covariance, a method that is often prone to
296 energy imbalance issues, i.e., the sum of the observed latent heat flux and sensible heat flux is
297 different from the available energy. We removed sites with an energy balance closure ratio (R_a)
298 values that were smaller than 0.60 or greater than 1.30. The R_a is calculated as the following.

$$299 \quad R_a = \frac{\lambda E + H}{R_n - G}$$

300 where H , R_n , and G denote the site level sensible heat flux, surface net radiation, and soil heat
301 flux respectively, all measured in W m^{-2} . In addition, a site affected by prolonged snow cover

302 was also removed. Finally, we preserved 180 flux sites (Figure 1; see also supporting information
303 in Table S1), which cover 13 different biome types and represent a wide range of climate
304 conditions.

305 Although FLUXNET2015 dataset also provides λE and H corrected for energy balance
306 enclosure by partitioning the residual energy between the two main dissipative heat fluxes on the
307 basis of the Bowen ratio (Twine et al., 2000), we used the original observations, since this
308 approach may fail in the case of short eddy covariance towers, that primarily sample small eddies.
309 Over a heterogeneous landscape, Bowen ratios of small eddies are different from those of large
310 eddies, which makes the energy balance closure correction factor hardly applicable (Foken,
311 2008). For GPP, we used the variable termed “GPP_NT_VUT_REF”, where NT indicates the
312 nighttime data-based method (Reichstein et al., 2005; Lasslop et al., 2010), VUT denotes the
313 varied friction velocity (u^*) threshold for filtering NEE data, and REF denotes the reference NEE
314 value, which is the value most similar to the other 39 ones out of 40 NEE estimates. For more
315 information concerning the derivation of GPP in FLUXNET2015 dataset, please refer to
316 <http://fluxnet.fluxdata.org/data/fluxnet2015-dataset/data-processing/>.



317
 318 Figure 1 Distribution of the 180 flux stations used for this study over the globe (some sites appear overlapped).
 319 These sites are categorized into 13 groups in terms of biome types: CRO_C3 = C3 crops; CRO_C4 = C4 crops;
 320 CSH = close shrub; DBF = deciduous broadleaf forest; DNF = deciduous needleleaf forest; EBF = every green
 321 broadleaf forest; ENF = evergreen needleleaf forest; GRA = grassland; MF = mixed forest; OSH = open shrub;
 322 SAV = savannah; WET = wetland; and WSA = woody savannah. Frequency of each biome is as follows:
 323 CRO_C3: 8, CRO_C3_C4: 8, CRO_C4: 2, CSH: 2, DBF: 21, DNF: 1, EBF: 14, ENF: 41, GRA: 34, MF: 8, OSH:
 324 12, SAV: 8, WET: 15 and WSA: 6. ‘CRO_C3_C4’ denotes a crop site where both C3 and C4 crops were grown
 325 for at least one growing season. The Projection and Geographic Coordinate Systems of this map are ‘World
 326 Robinson’ and ‘WGS-84’ and the central meridian is 0°.

327 We used daily data to calibrate and evaluate all models (see also section 2.3). Daily λE and
 328 GPP in the FLUXNET2015 dataset were the averages of hourly (or half-hourly, both hourly and
 329 half-hourly are referred to as hourly thereafter) values. However, if a large proportion of hourly
 330 values were unavailable, the daily value would be unreliable. For this reason, we removed daily
 331 λE or GPP data including more than 50% missing hourly values.

332 2.4.2 Remote sensing vegetation indices

333 Two vegetation indices, NDVI and EVI, were computed using the MODIS reflectance

334 bands.

$$335 \quad \text{NDVI} = \frac{\rho_{\text{NIR}} - \rho_{\text{RED}}}{\rho_{\text{NIR}} + \rho_{\text{RED}}}, \quad (10)$$

$$336 \quad \text{EVI} = 2.5 \frac{\rho_{\text{NIR}} - \rho_{\text{RED}}}{\rho_{\text{NIR}} + 6.0\rho_{\text{RED}} - 7.5\rho_{\text{BLUE}} + 1}, \quad (11)$$

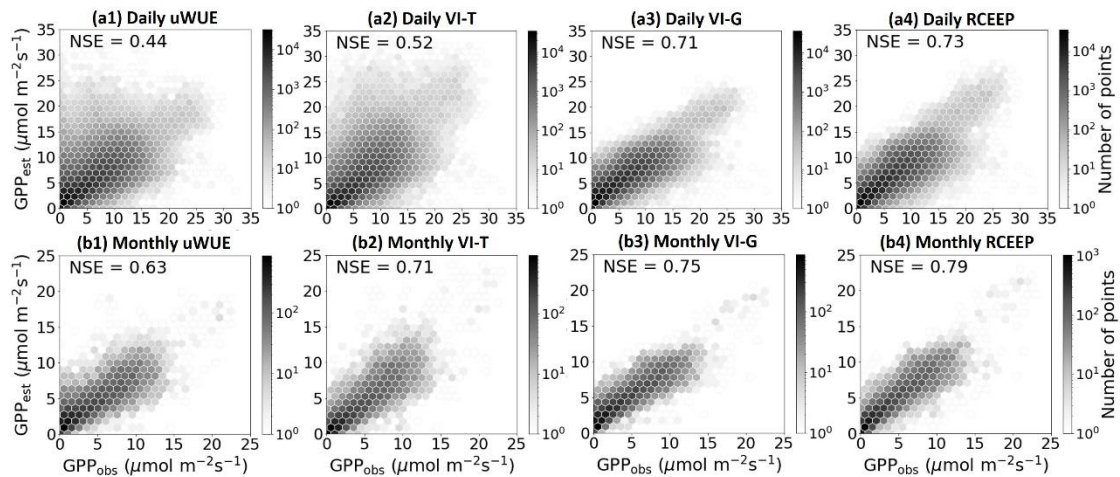
337 where ρ_{NIR} , ρ_{RED} , and ρ_{BLUE} denote the reflectance of near-infrared, red, and blue bands,
338 respectively, which were retrieved from the MOD09A1 product that has a temporal resolution of
339 8 days and spatial resolution of 500 m. We used the ‘Global Subsets Tool’, available on the
340 website of Oak Ridge National Laboratory (<https://modis.ornl.gov/data.html>), to retrieve the
341 reflectance data for each location from the pixel where the site is located. We removed
342 low-quality pixels (surface covered by snow or cloud) at each site and calculated NDVI and EVI
343 from the remaining data. The quality-controlled 8-day NDVI or EVI was then linearly
344 interpolated into daily values, using the nearest available data in the time sequence.

345 **3 Results**

346 **3.1 Cross-biome evaluation and analyses of RCEEP**

347 Cross-validations were carried out to compare the performances of the uWUE, VI-T, VI-G,
348 and RCEEP (Figure 2), parameterized with biome-specific factors (Appendix A) across all
349 biomes (Figure 1) on a daily and monthly scale. The three RS-based approaches, VI-T, VI-G, and
350 RCEEP, proved more efficient in reproducing daily and monthly GPP, featuring higher NSE
351 values compared to uWUE, in which T and D are approximated by ET and VPD, respectively
352 (Figure 3). On a daily scale, VI-T (NSE=0.52) and VI-G (NSE=0.71) featured better
353 performances than the original version of uWUE (NSE=0.44), which uses no VI-derived factors,
354 while RCEEP (using both NDVI- f_T and EVI- G_c) showed the best performance, with an NSE

355 value of 0.73. On a monthly scale, each model exhibited improved performance, while rankings
 356 in terms of NSE values were consistent, i.e., RCEEP > VI-G > VI-T > uWUE. Results provide
 357 evidence that incorporating both $NDVI-f_T$ and $EVI-G_c$ in the model can significantly contribute
 358 to improving the derivation of GPP on the basis of ET, at both daily and monthly scale.

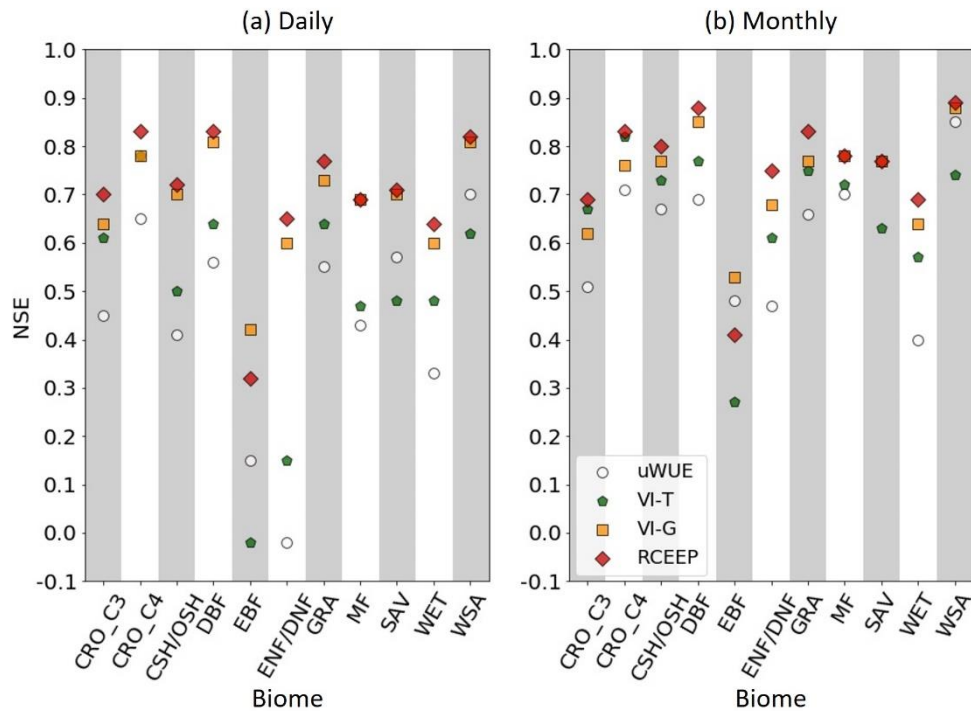


359 Figure 2 Comparison of Gross Primary Production estimated (GPP_{est}) by four models (uWUE, VI-T, VI-G, and
 360 RCEEP) with GPP observed at the FLUXNET ecosystem sites (GPP_{obs}) on a daily ((a1) – (a4)) and monthly ((b1)
 361 – (b4)) scale.

363 3.2 Biome-level evaluation and analyses of RCEEP

364 For each biome type, we again evaluated uWUE, VI-T, VI-G, and RCEEP (see also Table 1)
 365 parameterized with biome-specific parameters (Appendix A) with regard to reproducing GPP
 366 from ET on a daily and monthly scale (Figure 3 and Appendix B). Also, in this case, all four
 367 models featured better behavior at the monthly scale (Appendix B), since average monthly NSE
 368 values of the uWUE, VI-T, VI-G, and RCEEP were greater than daily values across all biome
 369 types, with the exception of CRO_C3 and C4 for VI-G, and RCEEP. Results highlight an
 370 inconsistent effect of incorporating $NDVI-f_T$ and $EVI-G_c$ on coupling ET and GPP over
 371 different biomes. VI-T and VI-G performed better than uWUE for most biome types (Figure 3)

372 and RCEEP was the best across all biomes except for EBF and SAV at both the daily and
 373 monthly scale (Appendix B). However, NDVI apparently failed to reflect the seasonal variations
 374 in f_T of EBF, since the inclusion of NDVI- f_T degraded the performances of both VI-T and
 375 RCEEP, while VI-G performed the best. On the other hand, VI-T and VI-G showed respectively
 376 worse and better performances than uWUE, in relation to SAV and WSA, while RCEEP
 377 performed similarly or better than VI-G (Figure 3 and Appendix B). Therefore, the inclusion of
 378 the sole NDVI- f_T act negatively on coupling ET and GPP as compared to uWUE, but it needs to
 379 be implemented along with EVI- G_c . As a whole, RCEEP can perform better than uWUE, VI-T,
 380 and VI-G over most biome types and reasonably calculate GPP from ET across all biome types
 381 with mean NSE values of 0.70 and 0.76 on a daily and monthly scale.

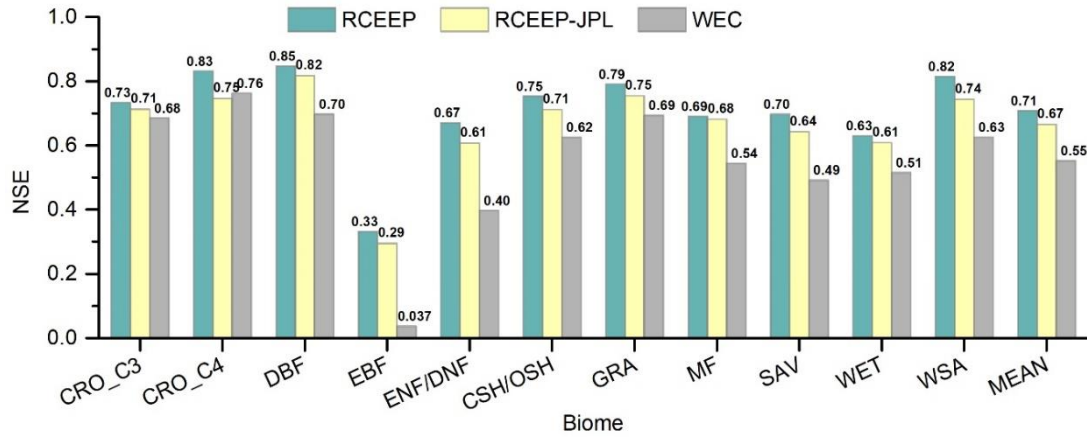


382
 383 Figure 3 NSE values for validating GPP_{est} by four models (uWUE, VI-T, VI-G, and RCEEP) against GPP_{obs}
 384 over 11 biome types on a daily (a) and monthly (b) scale. Here, we refer CSH/OSH or ENF/DNF as a unique
 385 biome type, because a single DNF and two CSH sites only were present in the dataset. Abbreviations of biome
 386 type are as in Figure 1.

387 3.3 Comparing RCEEP with RCEEP-JPL, WEC, and uWUE-Rg

388 The performances of RCEEP, RCEEP-JPL, and WEC parameterized with biome-specific
389 factors are shown in Figure 4 for each biome type, while Figure 5 presents biome-level
390 comparisons between RCEEP and uWUE-Rg. Both Figure 4 and Figure 5 revealed better
391 performances of RCEEP to reproduce GPP from ET on a daily scale for each biome type, on the
392 basis of significantly greater NSE values, compared with other approaches under investigation.
393 The biome level NSE values of RCEEP, RCEEP-JPL, and WEC are 0.71 (± 0.14), 0.67 (± 0.13),
394 and 0.55 (± 0.19), respectively, where values in parentheses are ± 1 standard deviation of NSE
395 across all biome types. These results indicated that NDVI- f_T provided more effective estimates
396 of the 'real' f_T than did the PT-JPL model. Although WEC used NDVI- f_T , it performed worse
397 than both RCEEP and RCEEP-JPL. This highlights the importance of a more reasonable
398 representation of stomatal effects in the relationship between ecosystem ET and GPP. Due to the
399 inclusion of the site-specific parameter, r , in WUE-Rg, we implemented WUE-Rg and RCEEP
400 with site-specific parameters at each flux site for a fair comparison between the two models. The
401 results of uWUE were also included in Figure 5 as a benchmark. The results showed that while
402 both uWUE-Rg and RCEEP can perform better than the uWUE, the latter yielded the best
403 performances across all biome types under investigation with larger mean values of NSE.

404



405

406

Figure 4 NSE values for RCEEP, RCEEP-JPL, and WEC with regard to reproducing GPP from ET over 11 biome

407

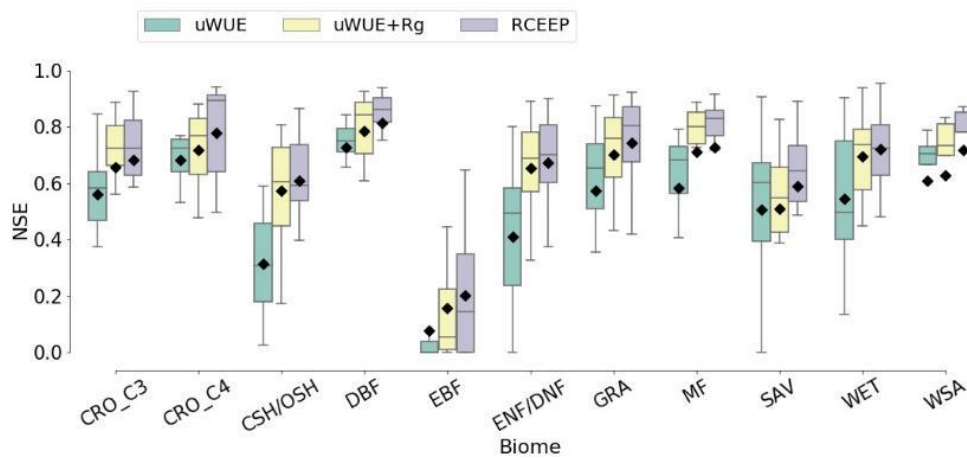
types on a daily scale. ‘MEAN’ denotes the NSE values averaged across all biome types. Details of RCEEP-JPL

408

and WEC can be found in Appendix D. All models are parameterized with biome-specified parameters. Refer to

409

Figure 1 for the explanation of each biome type.



410

411

Figure 5 Distributions of the site-level NSE values of three models (uWUE, uWUE-Rg, and RCEEP) to

412

reproducing GPP from ET based on site-specific parameters on a daily scale. Negative NSE values were forced

413

to be 0. The details of uWUE-Rg are presented in Appendix D. Data are retrieved from rain-free days’ of 160

414

sites with more than 300 observations. Four cropland sites (FR-Gri, IT-BCi, US-Ne2, and US-Ne3) shares

415

CRO_C4 and CRO_C3 biomes. Refer to Figure 1 for the explanation of the biome types.

416 4 Discussion

417 4.1 VI-derived f_T

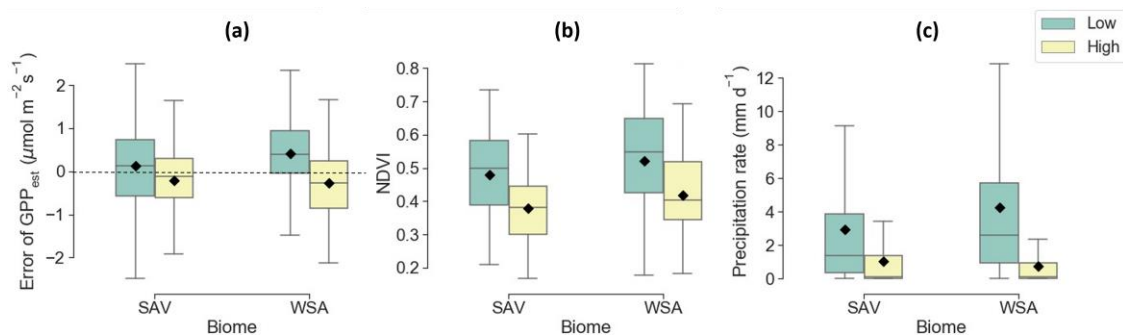
418

Assuming a constant f_T when building the relationships between ecosystem ET and GPP is

419 challenged by the variability of this parameter in relation to vegetation dynamics (Wang et al.,
420 2014; Zhou et al., 2016; Wei et al., 2017; Perez-Priego et al., 2018). We addressed this issue by
421 appraising f_T using NDVI-derived f_{PAR} and found that this approximation provides more
422 effective estimates than the complex ecophysiological ET model (Figure 4), PT-JPL, which is
423 driven by RS VIs and meteorological factors (Fisher et al., 2008). NDVI- f_T facilitated a better
424 relationship between ecosystem ET and GPP across all biome types except for EBF. However,
425 the usefulness of NDVI- f_T was impaired by the relatively high LAI value of dense canopies of
426 EBF, which is generally found in tropical and subtropical regions. Satellite-retrieved NDVI is
427 affected by canopy structure as well as by leaf chlorophyll content (Chl) (Wu et al., 2009; Croft
428 et al., 2017), thus NDVI of a thick canopy is dominated by Chl and may fail to represent the
429 variations in f_T .

430 We also found that NDVI- f_T seemed to act negatively on coupling ET and GPP of SAV and
431 WSA, since VI-T, which uses NDVI- f_T and approximates D by VPD, yielded smaller NSE
432 values than uWUE in reproducing GPP. On the other hand, NDVI- f_T always played a positive
433 role when used in combination with EVI- G_c (Figure 3). To find the reason for this interesting
434 result for SAV and WSA, we investigated the distributions of the errors in GPP_{est} from uWUE
435 at high and low VPD values over the two biome types (Figure 6), and found uWUE tended to
436 yield negative errors at low VPD and positive errors at high VPD values. Therefore, VPD could
437 be a driving force of the errors in uWUE. The leaf-to-air temperature difference can fall below
438 zero and show a negative correlation with VPD under unstressed conditions (Almeida, 1986;
439 Olufayo et al., 1993; Nelson and Bugbee, 2015), while savannah trees show comparable
440 well-watered conditions across both wet and dry seasons, due to their ability to access water

441 from deep soil layers (Herrera et al., 2012). Therefore, we speculate that the high VPD values,
 442 which generally appear in the dry season (Figure 6 (c)), could overestimate the actual value of D
 443 of SAV or WSA, and then degraded the performances of VI-T. For these biomes, high VPD
 444 values are also accompanied by low NDVI (Figure 6 (b)), which can amplify the errors induced
 445 by VPD in VI-T and thus result in worse performances. However, our study demonstrates the
 446 importance of including f_T in the model, as we found NDVI- f_T combined with EVI- G_c can
 447 lead to better performances of RCEEP compared with VI-G (see also Section 3.1 and 3.2).
 448 Perez-Priego et al. (2018) also supported our findings, who revealed significant seasonal
 449 variations in f_T , but its value rarely exceeded 80%, even in the case of a Mediterranean savannah
 450 ecosystem.
 451



452 Figure 6 Distributions of (a) errors of GPP_{est} from uWUE, (b) NDVI, and (c) precipitation rate on a monthly
 453 scale for high (green boxes) and low (yellow boxes) VPD values over two biomes (SAV and WSA). The solid
 454 black diamonds represent the mean values. Kolmogorov-Smirnov tests yielded significant differences in the
 455 distributions of each variable (errors of GPP_{est} , NDVI, and precipitation rate) between low and high-VPD values
 456 over each biome. The p -value of each test is smaller than 0.001. High and Low VPD values are divided by the
 457 50th percentile of monthly VPD values in each site-year.
 458

459 4.2 VI-derived G_c

460 The above discussion and the comparisons between RCEEP and VI-T/WEC revealed the

461 negative implications of approximating D by VPD. While previous studies discussed this issue
462 (Boese et al., 2017; Lin et al., 2018; Li et al., 2019), RCEEP addresses it by coupling ET and
463 GPP via VI-derived G_c (VI- G_c) rather than VPD. Efforts made by Boese et al. (2017) to
464 improve the performance of uWUE used a different approach, which was found to perform
465 worse than RCEEP (see also Section 3.3), however. As RS VIs were extensively used for
466 characterizing the photosynthetic features of vegetation (Yuan et al., 2010; Yuan et al., 2014; Yan
467 et al., 2015; Zhang et al., 2015), we speculate that the advantages of RCEEP are associated with
468 the ability of RS VIs to characterize biophysical features of terrestrial ecosystems, e.g. canopy
469 structure and greenness, which are important for quantifying photosynthesis of the vegetation
470 canopy, but cannot be successfully estimated in terms of VPD or R_g . Especially when T is highly
471 coupled to the atmosphere with a large value of G_c/G_a for the vegetation canopy, where G_a
472 denotes the aerodynamic conductance, T is hardly biophysically (i.e., G_c) controlled (Mallick et
473 al., 2016) and thus may be decoupled from photosynthesis. The success of using VIs discloses
474 then the potential of further improving the coupling of biome ET and GPP by considering more
475 biophysical features of ecosystems.

476 However, the use of VI- G_c may be impeded by the complicated effects of environmental
477 factors in addition to the RS VI. A more complicated formulation of G_c , the effects of multiple
478 environmental factors were accounted for, could be more useful. To clarify this issue, we
479 performed a comparison between the RCEEP version developed in this study and an alternative
480 version that uses a more complex formulation of G_c to account for various environmental
481 effects regarding estimating GPP from ET (Text S1). Interestingly, the result featured comparable
482 performances between the two RCEEP versions (see also Text S1), which revealed no tendencies

483 of the complex G_c to facilitate a better performance of RCEEP as compared to the VI- G_c .
484 Therefore, the simple formulation of G_c , as indicated by Eq.(6), is sufficient for quantifying GPP
485 using RCEEP along with ET. But this result can only be restricted to the applications of RCEEP.
486 Because the ability of ecosystem ET to indicate environmental controls (Baldocchi and Xu, 2007;
487 Ryu et al., 2008; Ma et al., 2015) on G_c can make up for the shortage of VI- G_c , which explains
488 the success of the application of RCEEP with VI- G_c .

489 4.3 The potential use of RCEEP and its limitations

490 RCEEP provides a straightforward approach to understanding the dynamics of GPP in
491 relation to ET. RS-based biophysical process models on coupled estimates of GPP and ET (Chen
492 and Liu, 2020), e.g. the Boreal Ecosystem Productivity Simulator (BEPS) (Chen et al., 2012),
493 Breathing Earth System Simulator (BESS) (Ryu et al., 2011; Jiang and Ryu, 2016), and the
494 coupled diagnostic biophysical model (PML-V2) (Zhang et al., 2019), incorporate process-based
495 modules to simulate GPP and then calculate T in terms of the first or second-order
496 Penman-Monteith equation (Monteith, 1965; Paw U and Gao, 1988) along with GPP-derived g_s
497 (Ball et al., 1987). Such a framework for simulating ET and GPP was also adopted in multiple
498 land surface models (De Kauwe et al., 2013; De Kauwe et al., 2015; Kala et al., 2015). These
499 models can reasonably simulate the variation in ET as a result of GPP but hardly show the
500 responses of GPP to the variations in ET. By contrast, RCEEP proved successful in calculating
501 GPP from ET and can thus provide a reliable and straightforward approach to understanding the
502 responses of GPP to the change of ET. Besides, RCEEP was proved to be more effective than an
503 analogous approach (see also Section 3.3), WEC, which is developed recently (Cheng et al.,

504 2017). To date, numerous methods have been developed to reasonably reproduce ET on a
505 regional or global scale (Michel et al., 2016; Chen and Liu, 2020; Fisher et al., 2020), therefore,
506 RCEEP can provide an easy approach to estimating regional or global-scale GPP by combing
507 these existing approaches, especially some thermal-driven models which can robustly compute
508 ET based on the energy balance theory in the absence of biome-specific parameters (Long and
509 Singh, 2012; Chen et al., 2013; Mallick et al., 2015; Mallick et al., 2016; Bhattarai et al., 2019).

510 Our analyses also evidenced that the performances of RCEEP are limited by the ability to
511 characterize the variations in f_T and G_c and could be potentially improved using more
512 appropriate RS factors. First, RCEEP can only be implemented on a daily or larger temporal
513 scale, because the sub-daily variations in G_c are dominated by meteorological factors, which
514 limits the use of VI- G_c on such a time scale. Second, we did not exhaust all the possible RS
515 factors, because this was beyond the scope of this study. Multiple VIs have been explored to
516 represent the biophysical features of vegetation (Wu et al., 2010; Yebra et al., 2013; Zhang et al.,
517 2015; Badgley et al., 2017). All these VIs have the potential of improving RCEEP. For example,
518 leaf chlorophyll concentration (Chl) is known to play an important role in regulating stomatal
519 conductance (Matsumoto et al., 2005), while some RS VIs are capable of characterizing the
520 variations in canopy Chl (Wu et al., 2009). Specific remotely sensed products are tightly
521 correlated with ecosystem photosynthesis. Satellite-retrieved vegetation near-infrared reflectance
522 (NIR_V) (Badgley et al., 2017) and solar-induced chlorophyll fluorescence (SIF) (Mohammed et
523 al., 2019) are further examples of RS retrieved parameters capable of characterizing
524 photosynthesis rate of terrestrial ecosystems for a wide range of biomes (Li et al., 2018; Badgley
525 et al., 2019; Zhang et al., 2020), as they are potentially useful for explaining part of the

526 photosynthesis dynamics that is independent of transpiration.

527 **5 Conclusion**

528 We developed RCEEP, an RS-driven approach aimed at coupling ecosystem ET and
529 photosynthesis (GPP) on a global scale. RCEEP did not use VPD to approximate D in the model
530 as did other generic methodologies but rather estimates ET on the basis of satellite EVI-derived
531 G_c . Besides, to remove the effect of soil evaporation, ET was scaled to T using a satellite
532 NDVI-derived f_T . As the newly established approach was developed as an improvement of
533 uWUE model, we compared the performances of RCEEP with uWUE and two additional
534 modified RS-driven versions (VI-T and VI-G), which only incorporate VI-derived f_T (VI- f_T) or
535 G_c (VI- G_c). Relative performances were assessed in terms of the NSE values for reproducing
536 GPP from ET on a daily and monthly scale over 180 flux sites covering 11 biome types over the
537 globe. In addition, considering the recent efforts to partitioning T from ET or representing more
538 meaningful relationships between ET and GPP on an ecosystem level, we furtherly compare
539 RCEEP with another three approaches modified from recent studies concerning estimating GPP
540 from ET. The results lead us to the following conclusions:

541 (a) VI-derived f_T and G_c can help to provide more meaningful relationships between
542 ecosystem ET and GPP, as the three RS-driven approaches, VI-T, VI-G, and RCEEP,
543 exposed more reasonable estimates of GPP compared to the uWUE, which relies on
544 VPD to approximate D

545 (b) RCEEP, incorporating both VI-derived f_T and G_c , yielded the best results and
546 performed better than uWUE over all biome types under investigation on a daily or, with

547 an exception of EBF, on a monthly scale.

548 (c) RCEEP featured reliable relationships between ecosystem GPP and ET, with NSE values
549 of 0.73 and 0.78 for reproducing daily and monthly GPP across all sites under
550 investigation.

551 (d) RCEEP was also found to perform better than another three models, RCEEP-JPL, WEC,
552 and uWUE-Rg, which are modified from recent studies, concerning estimating GPP
553 from ET.

554 The above results are encouraging in view of a reasonable relationship between
555 ecosystem-level ET and GPP and the coupled modeling of the two fluxes on a global scale,
556 because all RS data used in this study is worldwide available. We did not exhaust all the possible
557 RS factor which are potentially useful for representing plant biophysical features in developing
558 the RCEEP. The model can be further improved in future work, by introducing new RS factors to
559 characterize f_T and G_c and assessing a photosynthesis term that is independent of ET.

560

561 **Appendix**

562 Appendix A Biome-specific values of the estimated coefficients pertaining to the
 563 four approaches presented in Table 1, aimed at coupling ecosystem GPP and ET.

Biome type	uWUE	VI-T	VI-G	RCEEP
	Coefficients ^a			
	w	$w \cdot k_T$	$w \cdot \sqrt{k_G}$	$w \cdot \sqrt{k_G \cdot k_T}$
CRO_C3	3049	5060	3002	3808
CRO_C4	4689	6701	4249	5038
DBF	3820	4594	3078	3367
EBF	3243	4176	3171	3606
ENF/DNF	3165	4683	3435	4136
CSH/OSH	2179	3970	2220	2963
GRA	2698	3999	2717	3314
MF	3827	4838	3193	3562
SAV	3054	5745	2507	3602
WET	2060	3313	2326	2830
WSA	2866	4751	2376	3209
MEAN	3150	4712	2934	3585

564 ^a Refer to Figure 1 for the definition of each biome type. k_T is dimensionless, and the units of the other two
 565 coefficients are k_G : mol m⁻² s⁻¹; and w : μmol C (mol H₂O)⁻¹ kPa^{0.5}. But one cannot calculate the value of an
 566 individual multiplier using coefficients from different models. For example, we cannot divide the value of $w \cdot k_T$
 567 from VI-T by the w of uWUE, because the averaged effect of $k_T \cdot f_T$ in VI-T has been accounted for by the value
 568 of w of uWUE. Values of w , $w \cdot k_T$, $w \cdot \sqrt{k_G}$, and $w \cdot \sqrt{k_G \cdot k_T}$ can only be adopted for the formulations they
 569 belong to.

570 Appendix B NSE values of four models to reproduce GPP from ET over multiple
 571 biomes on a daily and monthly scale. MEAN denotes the average across all biome
 572 types. Please refer to Figure 1 for the explanation of each biome type.

Biome type	Daily				Monthly			
	uWUE	VI-T	VI-G	RCEEP	uWUE	VI-T	VI-G	RCEEP
CRO_C3	0.45	0.61	0.64	0.70	0.51	0.67	0.62	0.69
CRO_C4	0.65	0.78	0.78	0.83	0.71	0.82	0.76	0.83
DBF	0.56	0.64	0.81	0.83	0.69	0.77	0.85	0.88
EBF	0.15	-0.02	0.42	0.32	0.48	0.27	0.53	0.41
ENF/DNF	-0.02	0.15	0.60	0.65	0.47	0.61	0.68	0.75
CSH/OSH	0.41	0.50	0.70	0.72	0.67	0.73	0.77	0.80
GRA	0.55	0.64	0.73	0.77	0.66	0.75	0.77	0.83
MF	0.43	0.47	0.69	0.69	0.70	0.72	0.78	0.78
SAV	0.57	0.48	0.70	0.71	0.77	0.63	0.77	0.77
WET	0.33	0.48	0.60	0.64	0.40	0.57	0.64	0.69
WSA	0.70	0.62	0.81	0.82	0.85	0.74	0.88	0.89
MEAN	0.43	0.49	0.68	0.70	0.63	0.66	0.73	0.76

573 Appendix C The analytic water use efficiency (WUE) and inherent water use
574 efficiency (IWUE).

575 (1) Analytic WUE

576 [Medlyn et al. \(2011\)](#) proposed a theoretical stomatal conductance model based on the TOSB,
577 assuming that stomatal behavior was optimized for the photosynthesis limited by RuPB
578 generation. The TOSB and the expression of photosynthesis rate as limited by RuPB generation
579 ([Arneeth et al., 2002](#)) were coupled to derive the ‘optimal stomatal control model’.

$$580 \quad g_s = g_0 + 1.6 \left(1 + \frac{g_1}{\sqrt{D}} \right) \cdot \frac{A}{C_a}, \quad (C1)$$

581 where g_s denotes the stomatal conductance ($\text{mol m}^{-2} \text{s}^{-1}$); g_0 the minimum value of g_s ; D is
582 the leaf to air vapor pressure difference (kPa); A the net photosynthesis rate ($\mu\text{mol m}^{-2} \text{s}^{-1}$); C_a
583 the CO_2 concentration on the leaf surface ($\mu\text{mol mol}^{-1}$); and g_1 is a factor controlling the slope
584 of variations in g_s in relation to A . g_1 has an explicit physiological expression, $g_1 \propto \sqrt{\Gamma^* \lambda_m}$,
585 and is a key factor in Eq.(C1)), where Γ^* is the CO_2 compensation point in the absence of dark
586 respiration, and λ_m is the marginal water use efficiency. While assuming g_0 to be 0, integrating
587 Eq. (C1) with the transpiration rate expressed following the Fick’s law ([Beer et al., 2009](#); [Nobel,](#)
588 [2009](#)):

$$589 \quad T = g_s \cdot \frac{D}{P_a}, \quad (C2)$$

590 where T denotes the transpiration rate ($\text{mol m}^{-2} \text{s}^{-1}$), and P_a denotes the atmospheric pressure
591 (kPa); we can derive the following equation ([Medlyn et al., 2012](#)), representing the analytic
592 WUE.

$$593 \quad \text{WUE} = \frac{A}{T} = \frac{C_a \cdot P_a}{1.6(D + g_1 \cdot \sqrt{D})}, \quad (C3)$$

594 (2) IWUE

595 IWUE was proposed by Beer et al. (2009) to represent the relationship between
 596 ecosystem-level ET and GPP. The value of IWUE is supposed to remain constant for a given
 597 biome type under steady-state environmental conditions with a constant value of c_i/c_a . It was
 598 defined as follows (Beer et al., 2009):

$$599 \quad \text{IWUE} = \frac{\text{GPP} \cdot D}{T} = \frac{c_a \cdot (1 - c_i/c_a)}{1.6}, \quad (\text{C4})$$

600 where T and D are approximated by ET and VPD, respectively.

601 Appendix D Three approaches bridging ecosystem ET and GPP, modified from
 602 recent studies: comparisons with RCEEP.

603 (1) RCEEP-JPL: RCEEP incorporating f_T derived from the Priestley-Taylor Jet
 604 Propulsion Laboratory (PT-JPL)

605 The ET model Priestley-Taylor Jet Propulsion Laboratory (PT-JPL) (Fisher et al., 2008) is
 606 useful for computing f_T and then partitioning T from ET (Gu et al., 2018). PT-JPL is an
 607 RS-based ecophysiological ET model, which computes ET as a sum of T , E_i , and E_s , where E_i
 608 denotes the canopy interception evaporation. Therefore, f_T can be calculated based on the
 609 PT-JPL derived T (T_{JPL}) and ET (ET_{JPL}):

$$610 \quad f_T = \frac{T_{\text{JPL}}}{\text{ET}_{\text{JPL}}}, \quad (\text{D1})$$

611 Compared with f_T computed in terms of Eq. (8) along with NDVI in RCEEP, PT-JPL derived f_T
 612 (PT-JPL- f_T) explains more physical processes in partitioning T from ET and may have the
 613 potential of improving RCEEP. To clarify this issue, we compare the performances between an
 614 alternative RCEEP version incorporating PT-JPL- f_T (RCEEP-JPL) and the original version using
 615 NDVI- f_T . By substituting $k_T \cdot f_{\text{PAR}}$ with PT-JPL- f_T in RCEEP, we derive the alternative version

616 with PT-JPL- f_T , RCEEP-JPL, such that:

$$617 \quad \text{GPP} = \left(w \cdot \sqrt{k_G} \right) \cdot \sqrt{\text{sEVI} \cdot \frac{T_{\text{JPL}}}{\text{ET}_{\text{JPL}}} \cdot \text{ET} \cdot P_a^{-1}}, \quad (\text{D2})$$

618 (2) WEC: WUE and ET based carbon uptake model

619 WEC that estimates GPP using the analytic water use efficiency (WUE) (see also Appendix
620 C-(1)) (Medlyn et al., 2011) and ET was employed by Cheng et al. (2017), to understand the
621 response of the inter-annual dynamics of global carbon uptake in relation to the water cycle.

622 Such that:

$$623 \quad \text{GPP} = \frac{C_a \cdot P_a}{1.6(D + g_1 \cdot \sqrt{D})} \times T, \quad (\text{D3})$$

$$624 \quad T = \text{ET} \cdot f_T = \text{ET} \cdot f_{\text{PAR}} \cdot (1 - f_{\text{Ei}}), \quad (\text{D4})$$

625 where f_{Ei} denotes the proportion of E_i , to ET, and we fix f_{Ei} to 0 for rain-free days. Cheng et al.
626 (2017) computed f_{PAR} in terms of Beer's Law along with RS-derived LAI. In this study, we
627 estimated this variable on the basis of NDVI, according to Eq. (8). D in WEC is approximated by
628 VPD. The WEC is analogous to VI-T and also useful for bridging ecosystem ET and GPP, but it
629 adopts the framework of analytic WUE that is different from uWUE.

630 (3) uWUE-Rg: uWUE incorporating Solar radiation (R_g)

631 For representing a more meaningful relationship between ecosystem ET and GPP, Boese et
632 al. (2017) modified the uWUE by introducing an additional term, $r \cdot R_g$, where r is an empirical
633 factor and R_g denotes the solar radiation, to account for additional ET components, such that:

$$634 \quad \text{ET} = \frac{\text{GPP}}{\sqrt{D}} + r \cdot R_g, \quad (\text{D5})$$

635 where D is approximated by VPD. We could modify this equation to express GPP as a function

636 of ET:

$$637 \quad \text{GPP} = (\text{ET} - r \cdot R_g) \cdot \sqrt{D}, \quad (\text{D6})$$

638 We denoted this method as uWUE-Rg. The term $r \cdot R_g$ is associated with the variations in
639 stomatal conductance, equilibrium evaporation, and the difference between D and VPD and is
640 independent of uWUE term GPP/\sqrt{D} . This method is suitable to be applied at the site-scale due
641 to the significant spatial variability of the site-specific factor, r , a key parameter for a better
642 coupling of ET and GPP.

643 **Acknowledgments**

644 The authors would like to thank Prof. Torsten Sachs (Helmholtz Centre Potsdam, GFZ
645 German Research Centre for Geosciences) for his valuable comments on this paper. This
646 research is supported by the National Natural Science Fund of China (Grant Nos. 41901342,
647 31671585), the “Taishan Scholar” Project of Shandong Province, and Key Basic Research
648 Project of Shandong Natural Science Foundation of China (Grant No. ZR2017ZB0422).

649 Daily flux tower data used for the paper (see also Section 2.4.1 for Table S1) were retrieved
650 from the FLUXNET2015 Tier 2 dataset which is available through <https://fluxnet.fluxdata.org/>.

651 The site-level MOD09A1 product are available through the Oak Ridge National Laboratory
652 Distributed Active Archive Center (<https://modis.ornl.gov/data.html>). Detailed information of

653 crop rotations at each crop flux site is available through Bai et al. (2018). This work used eddy
654 covariance data acquired and shared by the FLUXNET community, including these networks:

655 AmeriFlux, AfriFlux, AsiaFlux, CarboAfrica, CarboEuropeIP, CarboItaly, CarboMont,
656 ChinaFlux, Fluxnet-Canada, GreenGrass, ICOS, KoFlux, LBA, NECC, OzFlux-TERN,

657 TCOS-Siberia, and USCCC. The FLUXNET eddy covariance data processing and harmonization
658 were carried out by the ICOS Ecosystem Thematic Center, AmeriFlux Management Project and
659 Fluxdata project of FLUXNET, with the support of CDIAC, and the OzFlux, ChinaFlux, and
660 AsiaFlux offices.

661 **References**

- 662 Almeida, J. A. P. (1986), Use of infrared thermometry to measure canopy-air temperature difference
663 at partial cover to assess crop water stress index, The University of Arizona, Tucson, US.
- 664 Arneth, A., J. Lloyd, H. Santrůcková, M. I. Bird, S. Grigoryev, Y. N. Kalaschnikov, G. Gleixner, and
665 E. D. Schulze (2002), Response of Central Siberian scots pine to soil water deficit and long-term
666 trends in atmospheric CO₂ concentration, *Global Biogeochemical Cycles*, 16(1), 5.1-5.13.
- 667 Badgley, G., C. B. Field, and J. A. Berry (2017), Canopy near-infrared reflectance and terrestrial
668 photosynthesis, *Science advances*, 3(3), e1602244.
- 669 Badgley, G., L. Anderegg, J. Berry, and C. Field (2019), Terrestrial Gross Primary Production: Using
670 NIR V to Scale from Site to Globe, *Global Change Biology*, 25.
- 671 Bai, Y., J. Zhang, S. Zhang, F. Yao, and V. Magliulo (2018), A remote sensing-based two-leaf canopy
672 conductance model: Global optimization and applications in modeling gross primary
673 productivity and evapotranspiration of crops, *Remote Sensing of Environment*, 215, 411-437.
- 674 Bai, Y., J. Zhang, S. Zhang, U. A. Koju, F. Yao, and T. Igbawua (2017), Using precipitation, vertical
675 root distribution, and satellite-retrieved vegetation information to parameterize water stress in a
676 Penman-Monteith approach to evapotranspiration modeling under Mediterranean climate,
677 *Journal of Advances in Modeling Earth Systems*, 9(1), 168-192.
- 678 Baldocchi, D. D., and L. Xu (2007), What limits evaporation from Mediterranean oak woodlands –
679 The supply of moisture in the soil, physiological control by plants or the demand by the
680 atmosphere?, *Advances in Water Resources*, 30(10), 2113-2122.
- 681 Ball, J. T., I. E. Woodrow, and J. A. Berry (1987), A Model Predicting Stomatal Conductance and its
682 Contribution to the Control of Photosynthesis under Different Environmental Conditions, in
683 *Progress in Photosynthesis Research: Volume 4 Proceedings of the VIIth International Congress*
684 *on Photosynthesis Providence, Rhode Island, USA, August 10–15, 1986*, edited by J. Biggins, pp.
685 221-224, Springer Netherlands, Dordrecht.
- 686 Beer, C., et al. (2009), Temporal and among-site variability of inherent water use efficiency at the
687 ecosystem level, *Global Biogeochemical Cycles*, 23(2), n/a-n/a.
- 688 Bhattarai, N., K. Mallick, J. Stuart, B. D. Vishwakarma, R. Niraula, S. Sen, and M. Jain (2019), An
689 automated multi-model evapotranspiration mapping framework using remotely sensed and
690 reanalysis data, *Remote Sensing of Environment*, 229, 69-92.
- 691 Boese, S., M. Jung, N. Carvalhais, and M. Reichstein (2017), The importance of radiation for
692 semiempirical water-use efficiency models, *Biogeosciences*, 14, 3015-3026.
- 693 Cavanaugh, M. L., S. A. Kurc, and R. L. Scott (2011), Evapotranspiration partitioning in semiarid

694 shrubland ecosystems: a two-site evaluation of soil moisture control on transpiration,
695 *Ecohydrology*, 4(5), 671-681.

696 Chen, J. M., and J. Liu (2020), Evolution of evapotranspiration models using thermal and shortwave
697 remote sensing data, *Remote Sensing of Environment*, 237, 111594.

698 Chen, J. M., G. Mo, J. Pisek, J. Liu, F. Deng, M. Ishizawa, and D. Chan (2012), Effects of foliage
699 clumping on the estimation of global terrestrial gross primary productivity, *Global*
700 *Biogeochemical Cycles*, 26(1).

701 Chen, X., Z. Su, Y. Ma, K. Yang, J. Wen, and Y. Zhang (2013), An Improvement of Roughness Height
702 Parameterization of the Surface Energy Balance System (SEBS) over the Tibetan Plateau,
703 *Journal of Applied Meteorology and Climatology*, 52(3), 607-622.

704 Cheng, L., L. Zhang, Y.-P. Wang, J. G. Canadell, F. H. S. Chiew, J. Beringer, L. Li, D. G. Miralles, S.
705 Piao, and Y. Zhang (2017), Recent increases in terrestrial carbon uptake at little cost to the water
706 cycle, *Nature Communications*, 8(1).

707 Collatz, G. J., J. T. Ball, C. Grivet, and J. A. Berry (1991), Physiological and environmental
708 regulation of stomatal conductance, photosynthesis and transpiration: a model that includes a
709 laminar boundary layer, *Agricultural and Forest Meteorology*, 54(2), 107-136.

710 Cowan, I. R., and G. D. Farquhar (1977), Stomatal function in relation to leaf metabolism and
711 environment, *Symposia of the Society for Experimental Biology*, 31, 471-505.

712 Croft, H., J. M. Chen, X. Luo, P. Bartlett, B. Chen, and R. M. Staebler (2017), Leaf chlorophyll
713 content as a proxy for leaf photosynthetic capacity, *Global change biology*, 23(9), 3513-3524.

714 De Kauwe, M. G., J. Kala, Y. S. Lin, A. J. Pitman, B. E. Medlyn, R. A. Duursma, G. Abramowitz, Y. P.
715 Wang, and D. G. Miralles (2015), A test of an optimal stomatal conductance scheme within the
716 CABLE land surface model, *Geoscientific Model Development*, 8(2), 431-452.

717 De Kauwe, M. G., et al. (2013), Forest water use and water use efficiency at elevated CO₂ : a
718 model-data intercomparison at two contrasting temperate forest FACE sites, *Glob Chang Biol*,
719 19(6), 1759-1779.

720 Drake, J. E., et al. (2017), Stomatal and non-stomatal limitations of photosynthesis for four tree
721 species under drought: A comparison of model formulations, *Agricultural and Forest*
722 *Meteorology*, 247, 454-466.

723 Fisher, J. B., K. P. Tu, and D. D. Baldocchi (2008), Global estimates of the land-atmosphere water
724 flux based on monthly AVHRR and ISLSCP-II data, validated at 16 FLUXNET sites, *Remote*
725 *Sensing of Environment*, 112(3), 901-919.

726 Fisher, J. B., et al. (2020), ECOSTRESS: NASA's Next Generation Mission to Measure
727 Evapotranspiration From the International Space Station, *Water Resources Research*, 56(4).

728 Foken, T. (2008), The energy balance closure problem: an overview, *Ecological Applications*, 18(6),
729 1351-1367.

730 Friedl, M. A. (1995), Modeling land surface fluxes using a sparse canopy model and radiometric
731 surface temperature measurements, *Journal of Geophysical Research: Atmospheres*, 100(D12),
732 25435-25446.

733 Gu, C., J. Ma, G. Zhu, H. Yang, K. Zhang, Y. Wang, and C. Gu (2018), Partitioning
734 evapotranspiration using an optimized satellite-based ET model across biomes, *Agricultural and*
735 *Forest Meteorology*, 259, 355-363.

736 Herrera, A., R. Urich, E. Rengifo, C. Ballestrini, A. González, and W. León (2012), Transpiration in a
737 eucalypt plantation and a savanna in Venezuela, *Trees*, 26(6), 1759-1769.

738 Idso, S. B. (1982), Non-water-stressed baselines: A key to measuring and interpreting plant water
739 stress, *Agricultural Meteorology*, 27(1), 59-70.

740 Idso, S. B., R. J. Reginato, and S. M. Farah (1982a), Soil- and atmosphere-induced plant water stress
741 in cotton as inferred from foliage temperatures, *Water Resources Research*, 18(4), 1143-1148.

742 Idso, S. B., R. J. Reginato, and J. W. Radin (1982b), Leaf diffusion resistance and photosynthesis in
743 cotton as related to a foliage temperature based plant water stress index, *Agricultural
744 Meteorology*, 27(1), 27-34.

745 Jackson, R. D., S. B. Idso, R. J. Reginato, and P. J. Pinter Jr (1981), Canopy temperature as a crop
746 water stress indicator, *Water Resources Research*, 17(4), 1133-1138.

747 Jasechko, S., Z. D. Sharp, J. J. Gibson, S. J. Birks, Y. Yi, and P. J. Fawcett (2013), Terrestrial water
748 fluxes dominated by transpiration, *Nature*, 496(7445), 347-350.

749 Jiang, C., and Y. Ryu (2016), Multi-scale evaluation of global gross primary productivity and
750 evapotranspiration products derived from Breathing Earth System Simulator (BESS), *Remote
751 Sensing of Environment*, 186, 528-547.

752 Jin, H., A. Li, J. Bian, X. Nan, W. Zhao, Z. Zhang, and G. Yin (2017), Intercomparison and validation
753 of MODIS and GLASS leaf area index (LAI) products over mountain areas: A case study in
754 southwestern China, *International Journal of Applied Earth Observation and Geoinformation*,
755 55, 52-67.

756 Kala, J., M. G. De Kauwe, A. J. Pitman, R. Lorenz, B. E. Medlyn, Y. P. Wang, Y. S. Lin, and G.
757 Abramowitz (2015), Implementation of an optimal stomatal conductance scheme in the
758 Australian Community Climate Earth Systems Simulator (ACCESS1.3b), *Geoscientific Model
759 Development*, 8(12), 3877-3889.

760 Krause, P., D. Boyle, and F. Bäse (2005), Comparison of Different Efficiency Criteria for Hydrologic
761 Models, *Advances in Geosciences*, 5.

762 Lasslop, G., M. Reichstein, D. Papale, A. D. Richardson, A. Arneeth, A. Barr, P. Stoy, and G.
763 Wohlfahrt (2010), Separation of net ecosystem exchange into assimilation and respiration using a
764 light response curve approach: critical issues and global evaluation, *Global Change Biology*,
765 16(1), 187-208.

766 Leuning, R. (1995), A critical appraisal of a combined stomatal-photosynthesis model for C3 plants,
767 *Plant, Cell & Environment*, 18(4), 339-355.

768 Li, X., P. Gentine, C. Lin, S. Zhou, Z. Sun, Y. Zheng, J. Liu, and C. Zheng (2019), A simple and
769 objective method to partition evapotranspiration into transpiration and evaporation at
770 eddy-covariance sites, *Agricultural and Forest Meteorology*, 265, 171-182.

771 Li, X., et al. (2018), Solar-induced chlorophyll fluorescence is strongly correlated with terrestrial
772 photosynthesis for a wide variety of biomes: First global analysis based on OCO-2 and flux
773 tower observations, *Global Change Biology*, 24(9), 3990-4008.

774 Lian, X., et al. (2018), Partitioning global land evapotranspiration using CMIP5 models constrained
775 by observations, *Nature Climate Change*, 8(7), 640-646.

776 Lin, C., P. Gentine, Y. Huang, K. Guan, H. Kimm, and S. Zhou (2018), Diel ecosystem conductance
777 response to vapor pressure deficit is suboptimal and independent of soil moisture, *Agricultural
778 and Forest Meteorology*, 250, 24-34.

779 Lloyd, J., and G. D. Farquhar (1994), ^{13}C discrimination during CO_2 assimilation by the terrestrial
780 biosphere, *Oecologia*, 99, 201-215.

781 Long, D., and V. P. Singh (2012), A Two-source Trapezoid Model for Evapotranspiration (TTME)

782 from satellite imagery, *Remote Sensing of Environment*, 121, 370-388.

783 Ma, N., Y. Zhang, Y. Guo, H. Gao, H. Zhang, and Y. Wang (2015), Environmental and biophysical
784 controls on the evapotranspiration over the highest alpine steppe, *Journal of Hydrology*, 529,
785 980-992.

786 Mallick, K., et al. (2015), Reintroducing radiometric surface temperature into the Penman-Monteith
787 formulation, *Water Resources Research*, 51(8), 6214-6243.

788 Mallick, K., et al. (2016), Canopy-scale biophysical controls of transpiration and evaporation in the
789 Amazon Basin, *Hydrol. Earth Syst. Sci.*, 20(10), 4237-4264.

790 Matsumoto, K., T. Ohta, and T. Tanaka (2005), Dependence of stomatal conductance on leaf
791 chlorophyll concentration and meteorological variables, *Agricultural and Forest Meteorology*,
792 132(1-2), 44-57.

793 Medlyn, B. E., R. A. Duursma, D. Eamus, D. S. Ellsworth, I. C. Prentice, C. V. M. Barton, K. Y.
794 Crous, P. De Angelis, M. Freeman, and L. Wingate (2011), Reconciling the optimal and
795 empirical approaches to modelling stomatal conductance, *Global Change Biology*, 17(6),
796 2134-2144.

797 Medlyn, B. E., R. A. Duursma, D. Eamus, D. S. Ellsworth, I. Colin Prentice, C. V. M. Barton, K. Y.
798 Crous, P. de Angelis, M. Freeman, and L. Wingate (2012), Reconciling the optimal and empirical
799 approaches to modelling stomatal conductance, *Global Change Biology*, 18(11), 3476-3476.

800 Medlyn, B. E., et al. (2017), How do leaf and ecosystem measures of water-use efficiency compare?,
801 *New Phytol*, 216(3), 758-770.

802 Michel, D., et al. (2016), The WACMOS-ET project – Part 1: Tower-scale evaluation of four
803 remote-sensing-based evapotranspiration algorithms, *Hydrology and Earth System Sciences*,
804 20(2), 803-822.

805 Mohammed, G., et al. (2019), Remote sensing of solar-induced chlorophyll fluorescence (SIF) in
806 vegetation: 50 years of progress, *Remote Sensing of Environment*, 231.

807 Monteith, J. L. (1965), Evaporation and environment, *Symposia of the Society for Experimental*
808 *Biology*, 19(19), 205-224.

809 Mott, K. A., and D. F. Parkhurst (1991), Stomatal responses to humidity in air and helox, *Plant, Cell*
810 *& Environment*, 14(5), 509-515.

811 Nash, J. E., and J. V. Sutcliffe (1970), River flow forecasting through conceptual models part I — A
812 discussion of principles, *Journal of Hydrology*, 10(3), 282-290.

813 Nelson, J. A., and B. Bugbee (2015), Analysis of Environmental Effects on Leaf Temperature under
814 Sunlight, High Pressure Sodium and Light Emitting Diodes, *PLoS One*, 10(10), e0138930.

815 Nobel, P. S. (2009), Chapter 8 - Leaves and Fluxes, in *Physicochemical and Environmental Plant*
816 *Physiology (Fourth Edition)*, edited, pp. 364-437, Academic Press, San Diego.

817 Olufayo, A., C. Baldy, P. Ruelle, and J. Konate (1993), Diurnal course of canopy temperature and leaf
818 water potential of sorghum (*Sorghum bicolor* L. Moench) under a Mediterranean climate,
819 *Agricultural and Forest Meteorology*, 64(3), 223-236.

820 Paw U, K. T., and W. Gao (1988), Applications of solutions to non-linear energy budget equations,
821 *Agricultural and Forest Meteorology*, 43(2), 121-145.

822 Perez-Priego, O., G. Katul, M. Reichstein, T. S. El-Madany, B. Ahrens, A. Carrara, T. M. Scanlon, and
823 M. Migliavacca (2018), Partitioning Eddy Covariance Water Flux Components Using
824 Physiological and Micrometeorological Approaches, *Journal of Geophysical Research:*
825 *Biogeosciences*, 123(10), 3353-3370.

826 Priestley, C. H. B., and R. J. Taylor (1972), On the Assessment of Surface Heat Flux and Evaporation
827 Using Large-Scale Parameters, *Monthly Weather Review*, *100*(2), 81-92.

828 Reichstein, M., et al. (2005), On the separation of net ecosystem exchange into assimilation and
829 ecosystem respiration: review and improved algorithm, *Global Change Biology*, *11*(9),
830 1424-1439.

831 Ryu, Y., D. D. Baldocchi, S. Ma, and T. Hehn (2008), Interannual variability of evapotranspiration
832 and energy exchange over an annual grassland in California, *Journal of Geophysical Research*,
833 *113*(D9).

834 Ryu, Y., et al. (2011), Integration of MODIS land and atmosphere products with a coupled-process
835 model to estimate gross primary productivity and evapotranspiration from 1 km to global scales,
836 *Global Biogeochemical Cycles*, *25*(4).

837 Sims, D., et al. (2005), Midday values of gross CO₂ flux and light use efficiency during satellite
838 overpasses can be used to directly estimate eight-day mean flux, *Agricultural and Forest
839 Meteorology*, *131*, 1-12.

840 Stoy, P., et al. (2019), Reviews and syntheses: Turning the challenges of partitioning ecosystem
841 evaporation and transpiration into opportunities, *Biogeosciences*, *16*, 3747-3775.

842 Twine, T. E., W. P. Kustas, J. M. Norman, D. R. Cook, P. R. Houser, T. P. Meyers, J. H. Prueger, P. J.
843 Starks, and M. L. Wesely (2000), Correcting eddy-covariance flux underestimates over a
844 grassland, *Agricultural and Forest Meteorology*, *103*(3), 279-300.

845 Wang, K., R. E. Dickinson, M. Wild, and S. Liang (2010), Evidence for decadal variation in global
846 terrestrial evapotranspiration between 1982 and 2002: 1. Model development, *Journal of
847 Geophysical Research*, *115*(D20).

848 Wang, L., S. P. Good, and K. K. Caylor (2014), Global synthesis of vegetation control on
849 evapotranspiration partitioning, *Geophysical Research Letters*, *41*(19), 6753-6757.

850 Wei, Z., K. Yoshimura, L. Wang, D. G. Miralles, S. Jasechko, and X. Lee (2017), Revisiting the
851 contribution of transpiration to global terrestrial evapotranspiration, *Geophysical Research
852 Letters*, *44*(6), 2792-2801.

853 Wu, C., Z. Niu, and S. Gao (2010), Gross primary production estimation from MODIS data with
854 vegetation index and photosynthetically active radiation in maize, *Journal of Geophysical
855 Research*, *115*(D12).

856 Wu, C., Z. Niu, Q. Tang, W. Huang, B. Rivard, and J. Feng (2009), Remote estimation of gross
857 primary production in wheat using chlorophyll-related vegetation indices, *Agricultural and
858 Forest Meteorology*, *149*(6-7), 1015-1021.

859 Yan, H., et al. (2015), Improved global simulations of gross primary product based on a new
860 definition of water stress factor and a separate treatment of C₃ and C₄ plants, *Ecological
861 Modelling*, *297*(0), 42-59.

862 Yang, P., R. Shibasaki, W. Wu, Q. Zhou, Z. Chen, Y. Zha, Y. Shi, and H. Tang (2007), Evaluation of
863 MODIS Land Cover and LAI Products in Cropland of North China Plain Using In Situ
864 Measurements and Landsat TM Images, *IEEE Transactions on Geoscience & Remote Sensing*,
865 *45*(10), 3087-3097.

866 Yebra, M., A. Van Dijk, R. Leuning, A. Huete, and J. P. Guerschman (2013), Evaluation of optical
867 remote sensing to estimate actual evapotranspiration and canopy conductance, *Remote Sensing of
868 Environment*, *129*, 250-261.

869 Yuan, W., et al. (2010), Global estimates of evapotranspiration and gross primary production based on

870 MODIS and global meteorology data, *Remote Sensing of Environment*, 114(7), 1416-1431.

871 Yuan, W., et al. (2014), Global comparison of light use efficiency models for simulating terrestrial
872 vegetation gross primary production based on the LaThuile database, *Agricultural and Forest
873 Meteorology*, 192-193, 108-120.

874 Zhang, K., J. S. Kimball, Q. Mu, L. A. Jones, S. J. Goetz, and S. W. Running (2009), Satellite based
875 analysis of northern ET trends and associated changes in the regional water balance from 1983 to
876 2005, *Journal of Hydrology*, 379(1-2), 92-110.

877 Zhang, Q., Y.-B. Cheng, A. I. Lyapustin, Y. Wang, X. Zhang, A. Suyker, S. Verma, Y. Shuai, and E. M.
878 Middleton (2015), Estimation of crop gross primary production (GPP): II. Do scaled MODIS
879 vegetation indices improve performance?, *Agricultural and Forest Meteorology*, 200, 1-8.

880 Zhang, Y., D. Kong, Q. Zhang, and Y. Yang (2019), Coupled estimation of 500m and 8-day resolution
881 global evapotranspiration and gross primary production in 2002–2017, *Remote Sensing of
882 Environment*, 222, 165–182.

883 Zhang, Y., C. Song, G. Sun, L. E. Band, S. McNulty, A. Noormets, Q. Zhang, and Z. Zhang (2016),
884 Development of a coupled carbon and water model for estimating global gross primary
885 productivity and evapotranspiration based on eddy flux and remote sensing data, *Agricultural
886 and Forest Meteorology*, 223, 116-131.

887 Zhang, Z., et al. (2020), Reduction of structural impacts and distinction of photosynthetic pathways in
888 a global estimation of GPP from space-borne solar-induced chlorophyll fluorescence, *Remote
889 Sensing of Environment*, 240.

890 Zhou, S., B. Yu, Y. Huang, and G. Wang (2014), The effect of vapor pressure deficit on water use
891 efficiency at the subdaily time scale, *Geophysical Research Letters*, 41(14), 5005-5013.

892 Zhou, S., B. Yu, Y. Huang, and G. Wang (2015), Daily underlying water use efficiency for AmeriFlux
893 sites, *Journal of Geophysical Research: Biogeosciences*, 120(5), 887-902.

894 Zhou, S., B. Yu, Y. Zhang, Y. Huang, and G. Wang (2016), Partitioning evapotranspiration based on
895 the concept of underlying water use efficiency, *Water Resources Research*, 52(2), 1160-1175.

896

897